

37 showed lower inhibitory effects. To discern between Oatp1d1 substrates and inhibitors, results were
38 complemented by Michaelis–Menten kinetics and chemical analytical determinations of MCs uptake,
39 along with molecular docking studies performed using the developed zebrafish Oatp1d1 homology
40 model. Therefore, our study showed that Oatp1d1-mediated transport of MCs could be largely
41 dependent on their basic physicochemical properties, with log P_{OW} being the most obvious
42 determinant. Finally, apart from determination of the chemical composition of cyanobacterial blooms,
43 a reliable risk assessment should take into account the interaction of identified MC congeners with
44 Oatp1d1 as their primary transporter, and herewith we demonstrated that such a comprehensive
45 approach could be based on the use of highly specific *in vitro* models, accompanied by chemical
46 assessment and *in silico* molecular docking studies.

47

48 **Keywords:** microcystins; zebrafish Oatp1d1; kinetics determinations; substrates vs. inhibitors;
49 chemicaly analytical determinations; molecular docking

50

51 **1. Introduction**

52 Cyanobacteria are marine, freshwater or terrestrial photosynthetic bacteria that possess the ability to
53 produce a wide variety of secondary metabolites which enable them to modify their habitats and
54 thrive under diverse environmental stress conditions (Sivonen and Jones, 1999; Dittmann et al.,
55 2013). Cyanobacterial secondary metabolites are in most cases highly bioactive substances, and some
56 of them, called cyanotoxins, have been shown to present a significant risk to livestock, fish, other
57 aquatic organisms and human health upon their release into aquatic environments during so-called
58 harmful algal blooms (HABs). HABs are a phenomenon that typically occurs in aquatic ecosystems
59 in conditions of high nutrient input, eutrophication and increased temperature. They can be formed
60 by various genera of cyanotoxin-producing cyanobacteria (toxic strains) and non-cyanotoxin-
61 producing cyanobacteria (non-toxic strains) (D'Anglada et al., 2016; Zohdi and Abbaspour, 2019).
62 Considering the increased occurrence of cyanobacterial blooms, as well as human and animal
63 poisonings (Wang et al., 2021), much effort has been put into revealing the toxic effects and molecular
64 mechanisms of cyanobacterial toxicity (reviewed e.g., in Ferrão-Filho and Kozłowski-Suzuki, 2011;
65 Buratti et al., 2017). Among the many types of cyanotoxins, microcystins (MCs) are the most
66 dominant in cyanobacterial blooms. They have been shown to be highly toxic and they are often
67 associated with hepatotoxicity, nephropathy, neurotoxicity and other severe toxic effects, particularly
68 upon harmful algal blooms (Chen et al., 2009). MCs are highly diverse in terms of molecular size,
69 structure and physicochemical properties, with almost 280 congeners identified so far (Bouaïcha et
70 al., 2019). A typical MC structure consists of seven amino acids in a ring formation (cyclic
71 heptapeptides) with an obligatory presence of a β -amino acid side chain (ADDA group), and their
72 nomenclature is primarily based on two variable amino acids that are always occupied by L-amino
73 acids (Fig. S1 in Supplementary Material).

74 The mechanisms of toxicity related to MCs are diverse, and the most studied one includes interactions
75 with protein phosphatases PP1 and PP2A which in turn lead to the hyperphosphorylation of cellular
76 proteins, DNA destruction, inflammation, apoptosis, hepatic hemorrhage and necrosis (MacKintosh
77 et al., 1990). Induction of oxidative stress and interaction with cellular uptake mechanisms is also
78 associated with exposure to MCs, causing cytoskeletal disruption, cancer cell invasion and DNA
79 damage (reviewed e.g., in McLellan and Manderville, 2017; Bouaïcha et al., 2019). As shown in
80 several studies, the toxic potential of MCs depends on their toxicodynamics and toxicokinetics
81 properties, and along with their inhibitory potency towards serine/threonine protein phosphatases
82 (PPs), their uptake kinetics is probably a key determinative of the organ and/or species-specific
83 toxicity of individual congeners. Interaction of MCs with serine/threonine PPs has been extensively
84 addressed in numerous studies and data show that most toxic congeners frequently found in HABs
85 have similar potency in the inhibition of PP1, PP2, and PP4-6, typically showing IC₅₀ values in the
86 range of 0.1–1 nM (Bouaïcha et al., 2019). The inhibition of the PPs activity by MCs results primarily

87 from non-covalent interactions, although covalent interaction does occur between MCs and the
88 catalytic sub-units of PPs. However, formation of the covalent bond occurs slowly, and is not essential
89 for the inactivation of the PPs by MCs (Craig et al., 1996; Hastie et al., 2005; Perreira et al., 2011).
90 Considering the uptake of MCs in various cells and tissues of mammals and fish species, it is mostly
91 mediated by organic anion-transporting polypeptides (OATPs in humans and rodents; Oatps in fish
92 and other species) (Fischer et al., 2010; Niedermeyer et al., 2014, Steiner et al., 2015). OATPs/Oatps
93 are transmembrane proteins that typically consist of 12 transmembrane domains, and their primary
94 physiological role appears to be the hepatic transport of steroid and thyroid hormones, bile salts,
95 prostaglandins and oligopeptides. However, they have been shown to be involved in the transport of
96 endo- and xenobiotics. They are typically polyspecific and expressed in most tissues, with specific
97 members dominantly expressed in toxicologically important organs as the liver or kidney (Hagenbuch
98 and Meier, 2003; Popović et al., 2010). Transport of MCs has been demonstrated for human
99 OATP1B1 and OATP1B3, and rat and mice OATP1B2 (Fischer et al., 2005; Komatsu et al., 2007).
100 Members of the Oatp1 family were shown to interact with MCs in fish species such as the little skate,
101 rainbow trout and zebrafish. Considering tissue distribution of Oatp1 transcripts, the level of their
102 expression, and specificity towards MC congeners, the Oatp1d1 appears to be dominant transporter
103 of MCs (Meier-Abt et al., 2007; Bury et al., 1998; Bieczynski et al., 2014; Steiner et al., 2015;
104 Faltermann et al., 2016).

105 From the ecotoxicological perspective, it is important to emphasize that the studies done so far
106 indicate that the rate of MCs uptake, determined e.g., in zebrafish as a cyprinid fish model, varies for
107 different congeners which may partially explain the observed differences in their toxic potential.
108 Furthermore, as Oatp1d1 transporter appears to be highly relevant for uptake of MCs in zebrafish, it
109 is important to better understand the potency and type of interaction of structurally and chemically
110 different MC congeners with fish Oatp1d1. If the interaction of various MCs with Oatp1d1 is
111 significantly different, both in terms of their potency and type of interaction, the presence of highly
112 toxic congeners in HABs might not represent high ecological risk if their Oatp1d1 transport is low.
113 On the contrary, the presence of less toxic congeners with high rate of Oatp1d1 mediated transport
114 could be highly deleterious. Therefore, in this study we addressed this topic using a zebrafish model:
115 six MC congeners of varying physicochemical properties (MC-LR, -RR, -YR, -LW, -LF, -LA) that
116 are frequently found in HABs were tested for their interaction with a target transporter using HEK
117 293T cells transiently or stably expressing zebrafish Oatp1d1 cloned from zebrafish liver. Results of
118 interaction studies were further verified by chemical analytical determinations of MC uptake in
119 transfected cells, and by molecular docking studies performed for specific congeners.

120

121

122 **2. Materials and methods**

123 *2.1. Chemicals*

124 Model fluorescent substrate Lucifer yellow (LY), Trypsin-EDTA solution and Hepes were purchased
125 from Sigma-Aldrich, St. Louis, MO, USA. Dulbecco's Modified Eagle's Medium (DMEM) (Powder,
126 High Glucose, Pyruvate), Fetal Bovine Serum (FBS) and Phosphate Buffer Saline (PBS) were
127 purchased from Gibco Invitrogen, Life technologies, CA, USA. The other solvents and salts used
128 were of the highest analytical grade and purchased from Kemika, Zagreb, Croatia.

129 *2.2. Microcystins standards*

130 Six microcystin (MC) congeners were purchased from Enzo Life Sciences: MC-LR, -RR, -YR, -LW,
131 -LF, and -LA. Stock standard solutions were prepared in methanol and stored at -80 °C.
132 Concentrations of stock standard solutions made for analytical LC-MS analyses were 1 µg/µL, while
133 the stock concentrations used for bioassays were 10 mM (-LR) and 1 mM (-RR, -YR, -LW, -LF, and
134 -LA). For LC-MS analyses, stock standards were diluted 1/100 in methanol (final concentrations 10
135 ng/µL). An overview of the structure and basic chemical and physical properties of microcystin
136 congeners tested in this study has been provided in the Supplementary Material (Table S1, Fig. S1).

137
138 *2.3. Oatp1d1 transport activity measurements*

139 Interaction of selected MCs with zebrafish Oatp1d1 transporter was determined by using the uptake
140 transport assay with transiently transfected human embryonic kidney HEK293T cells overexpressing
141 the Oatp1d1 uptake transporter cloned from zebrafish liver, as described previously (Popovic et al.,
142 2013; Maric et al., 2017). Briefly, HEK293T cells overexpressing zebrafish Oatp1d1 were co-
143 exposed for 5 min to serial dilutions of MCs and LY as a model substrate, and the rate of Oatp1d1
144 LY transport was determined. MCs were tested in the concentration range from 0.02 to 100 µM, the
145 final concentration of Oatp1d1-specific substrate LY used in the assays was 10 µM, and the maximal
146 amount of solvents (MeOH for MCs, dimethyl sulfoxide (DMSO) for LY) never exceeded 0.1%.
147 After incubation, the cells were washed twice with an ice-cold incubation medium (250 µL/well) and
148 incubated with 250 µL/well of 0.1% sodium dodecyl sulfate (SDS) for 30 min at 37 °C for cell lysis.
149 Fluorescence of transport specific substrates was measured in 96-well black microplates using a
150 microplate reader (Infinite M200, Tecan, Salzburg, Austria) at specific wavelengths of 425/540 nm.
151 The eukaryotic vector pcDNA3.1(+)/His without cloned genes (mock-transfected cells) was also
152 transfected into the HEK293T cells in order to determine non-transporter specific uptake. Oatp1d1-
153 transfected cells exposed only to incubation medium were used as an additional negative control.

154
155 *2.4. Type of interaction of MCs with Oatp1d1 transporter*

156 *2.4.1. Michaelis-Menten transport kinetics*

157 Stable expression of zebrafish Oatp1d1 in genetically engineered HEK293 Flp-In cells (Thermo
158 Fisher Scientific, Waltham, USA) was achieved using a non-clonal selection, by targeted integration

159 of the *oatp1d1* sequence subcloned into integration vector pcDNA5/FRT (Thermo Fisher Scientific,
160 Waltham, USA) with combination of restriction enzymes HindIII/XhoI. pcDNA5/FRT/Oatp1d1
161 constructs were specifically targeted into the genome of the Flp-InTM-293 cells following the
162 manufacturer's instructions, using basically the same protocol as described in Lončar and Smital
163 (2018). Zebrafish Oatp1d1 stable transfectants were functionally verified by determination of the
164 uptake rate of model fluorescent substrate LY in comparison to mock-transfected cells, and the stable
165 cell line was further maintained in the same conditions as regular HEK293T cells.

166 For the type of interaction experiments, HEK293T Flp-In/Oatp1d1 cells were seeded in 96-well
167 plates at a density of 5 or 8 x 10⁵ cells/mL in a final volume of 125 µL/well. Forty-eight hours after
168 seeding, the growth medium was extracted from the cells and 100 µL/well of incubation medium
169 (145 mM NaCl, 3 mM KCl, 1 mM CaCl₂, 0.5 mM MgCl₂, 5 mM D-glucose, and 5 mM HEPES) was
170 added. Preincubation lasted for 10 min after which 25 µL/well of medium was removed. The activity
171 of the Oatp1d1 transporter was measured by exposing the cells to six concentrations of model
172 substrate LY (5-300 µM) and two to three concentrations of MCs ranging from 0.05 – 100 µM. The
173 exposure volume of LY and MCs added to the cells was 25 µL/well. The maximal amount of DMSO
174 and MeOH used as solvents in all of the tested samples never exceeded 0.1%. A shift in the K_m and
175 V_{max} values of Oatp1d1 transport was determined after 15 min incubation of LY with MCs, as the
176 uptake of LY is linear during the first 15 min of incubation (Popovic et al., 2013). After incubation,
177 the cells were washed twice with 125 µL/well of cold incubation medium and subsequently incubated
178 with 125 µL/well of 0.1% SDS for 30 min at 37 °C for cell lysis. As a control, the activity of the
179 Oatp1d1 transporter in HEK293T Flp-In/Oatp1d1 cells was measured in the presence of model
180 substrate LY only (six concentrations). The uptake into HEK293T Flp-In/mock cells was subtracted
181 to obtain transporter-specific uptake. The K_m increase and no changes in V_{max} indicated MCs as
182 substrates (competitive inhibition); no significant changes in K_m and reduced V_{max} pointed to non-
183 competitive inhibition; and reduced K_m and V_{max} indicated un-competitive inhibition. The
184 measurements were done in duplicates and conducted in two to three independent experiments, and
185 results of representative experiments are shown in the Results section. To obtain a linear calibration
186 curve, the fluorescent dye LY was dissolved in 0.1% SDS, in the cell matrix dissolved in 0.1% SDS
187 and in the incubation medium to obtain the linear calibration curves. Bradford assay was used to
188 measure total protein concentration (Bradford, 1976). Based on total protein measurements and the
189 obtained linear calibration curves, the uptake rate of LY was calculated and expressed as nmol of
190 substrate per µg of protein per minute.

191

192

193

2.4.2. Chemical analytical verification of the type of interaction

194 The MCs that showed significant interaction with zebrafish Oatp1d1 were preliminarily classified as
195 substrates (competitive inhibitors) or non/un-competitive inhibitors based on results of Michaelis-
196 Menten kinetics experiments and were then further verified on the type of interaction by exposure of
197 HEK293T Flip-In/Oatp1d1 stable transfectants and mock-transfected cells to MCs followed by a
198 chemical analytical determination of the intracellular accumulation of the tested MCs by LC-MS
199 analyses. Cells were seeded in 24-well plates at 8×10^5 cells/mL density in a final volume of 500
200 μ L/well and 48 h after seeding were exposed to different concentrations of MCs. After removing the
201 growth medium above the cells, preincubation was initiated by adding 400 μ L/well of incubation
202 medium. Ten minutes later, HEK293T Flip-In/Oatp1d1 cells were exposed to three MC
203 concentrations selected based on the initial transport activity determinations: 0.1, 0.5 and 1 μ M for
204 MC-LW and -LF; 0.5, 1 and 5 μ M for MC-LA and -YR; 5, 20 and 50 μ M for MC-LR. The maximal
205 amount of MeOH used as solvent in all of the tested samples never exceeded 0.5%. Incubation with
206 MCs lasted for 30 min after which cells were washed two times with 500 μ L/well of incubation
207 medium. The cells were then incubated in 500 μ L/well of MeOH for 30 min at 37 °C in order to
208 permeabilize the cells and extract the accumulated MCs. HEK293T Flip-In/mock cells were also
209 exposed to the same concentrations of MCs in order to discern between transporter-specific and
210 passive uptake of the tested MCs. After the final incubation in MeOH, cells were manually scraped
211 from the bottom of the wells and technical duplicates from each concentration were merged into a
212 single tube. Samples were then centrifuged for 5 min at 1000 x g to remove cellular debris and
213 proteins. Supernatant was transferred to a conical tube and 10 mL of MeOH was added. Samples
214 were centrifuged for 5 min at 1000 x g, transferred to glass tubes and MeOH was evaporated under a
215 nitrogen stream using a TurboVap system (Caliper Life Sciences, Hopkinton, MS, USA) at 40 °C
216 until dryness. Residual dry matter was dissolved in 250 μ L of MeOH.

217 The prepared final solutions from the assays were analyzed by liquid chromatography-mass
218 spectrometry (LC/MS). All analyses were performed using a Waters Acquity ultra-performance
219 liquid chromatography (UPLC, Waters Corp., Milford, Massachusetts, USA) coupled to a Q-TOF
220 Premier quadrupole-time-of-flight mass spectrometer (QTOF-MS; Waters Corp., Milford,
221 Massachusetts, USA) equipped with an electrospray ionization source. The UPLC system was
222 equipped with a 1.7 μ BEH C18 column (100 x 4 mm) for chromatographic separation of MCs. The
223 eluents A and B were acetonitrile with 0.1 % formic acid (v/v) and water with 0.1 % formic acid
224 (v/v), respectively, and the flow rate was 0.4 ml/min. The sample acquisition was performed in
225 positive ionization mode in the m/z range from 50 to 1100 Da. The details of the mass spectrometric
226 settings were described elsewhere (Terzic and Ahel, 2011). For the quantitative assessment of
227 individual MCs, the acquired full scan chromatograms were reconstructed using accurate masses of
228 the corresponding $[M+H]^+$ ions of MCs as follows: MC-LR (m/e 995.557), MC-YR (m/e 1045.536),
229 MC-LW (m/e 1025.535), MC-LF (m/e 986.524) and MC-LA (m/e 910.493). The representative

230 chromatograms are given in the Supplementary Material (Fig. S1). The confirmation of peak
231 identities as well as the quantitative assessment was performed using authentic standards as described
232 above.

233

234 2.5. Homology modelling and molecular docking studies

235 Biovia Discovery Studio Client v18.1. (Dassault Systèmes, Vélizy-Villacoublay, France)
236 implemented Build Homology Models protocol was used to construct Oatp1d1 homology model
237 based on alignment of the model sequence and the template structure - crystal structure of the
238 glycerol-3-phosphate transporter from *Escherichia coli* (PDB ID: 1pw4) (Meier-Abt et al., 2006,
239 Huang et al., 2003). Build Homology Models protocol uses the MODELER (Sali and Blundell, 1993)
240 automodel to build homology models. To build an Oatp1d1 homology model, the input sequence
241 alignment between the model sequence of Oatp1d1 and the sequence of glycerol-3-phosphate
242 transporter was obtained using the Align Sequences protocol (Sequence Identity: 11.6 %, Sequence
243 Similarity: 34,3 %). The alignment was analyzed and long insertions that could not be modeled
244 correctly were excised from the alignment in order to obtain a reliable model. The N-terminal variable
245 region and the large extracellular and intracellular loops/regions that were judged to be unreliable and
246 not important for ligand binding were excised.

247 The remaining parameters in the Parameters Explorer of the Build Homology Models protocol were
248 set as follows: Cut Overhangs was set to True to cut the terminal residues of the input model sequence
249 that were not aligned with the templates; Number of Models was set to 10 to specify the number of
250 models to create from an initial structure with Optimization Level set to High to define the proportion
251 of molecular dynamics with simulated annealing to perform. As to building refinement models on
252 detected loop regions, i.e., the model sequence regions of at least 5 residues length which are not
253 aligned with the template, Refine Loops was set to True. Build Homology Models protocol uses the
254 DOPE (Discrete Optimized Protein Energy) (Shen and Sali, 2006) method to refine loops. Refine
255 Loops Number of Models was set to 5 to define the number of models to be created by loop
256 optimization, and Refine Loops Optimization Level was set to Low to define the number of models
257 to be created by loop optimization. Refine Loops with Use Discrete Optimized Protein Energy
258 (DOPE) Method was set to High Resolution. After running Build Homology Models protocol, the
259 Best Model Structure Superimposed to Templates was selected from the generated output models for
260 the final three-dimensional model structure of Oatp1d1. Finally, the selected model was manually
261 adjusted and minimized using the Smart Minimizer algorithm. The dielectric constant used to
262 minimize the Oatp1d1 model was set to 2 corresponding to the dielectric properties of saturated
263 hydrocarbons as instructed when modelling a membrane system.

264 Microcystin congeners to be docked in the homology model of Oatp1d1 were created with
265 ChemBio3D Ultra 13.0 (PerkinElmer, Inc., Waltham, MA, USA) and minimized using the Minimize

266 Ligands protocol implemented in Biovia Discovery Studio Client v18.1. Flexible Docking protocol
267 (Koska et al., 2008) was used for the molecular docking study with flexible amino acid side-chains
268 which comprises the following steps: ChiFlex receptor conformations calculation, ligand
269 conformations creation, LibDock docking of the ligand into active protein conformation sites, poses
270 clustering to remove similar ligand poses, ChiRotor protein conformations rebuilding by refining
271 selected protein side-chains in the presence of the rigid ligand, and a final CDOCKER ligand
272 refinement. The selected homology model of Oatp1d1 was used as the rigid receptor, while the
273 binding site within the homology models was defined by a sphere ($r=25 \text{ \AA}$) surrounding the central
274 pore. The rest of the parameters included in the FlexibleDocking protocol were set as follows.
275 Maximum number of processed protein conformations was set to 100; Minimum angle, i.e. torsion
276 angle cutoff (degrees) to determine whether the two side-chain χ_1 angles are the same or not, was
277 set to 30; Maximum number of residues for generating side chain conformations was set to 16 and
278 these were the following: Met37, Lys38, Glu63, Ile70, Arg172, Glu176, Tyr199, Ile203, Val206,
279 Val347, Phe350, Ile351, Ile354, Leu575, and Arg578; Conformation Method, i.e. algorithm for
280 generating ligand conformations, was set to BEST; Maximum number of conformations to be created
281 was set to 255; Energy Threshold, i.e. conformations of separate isomers are created inside this
282 relative energy threshold (kcal/mol), was set to 20. LibDock ligand docking parameters inside
283 FlexibleDocking protocol were set as follows: Number of Hotspots, i.e. number of polar or apolar
284 receptor hotspots for conformer matching and Max Number to Save were set to 100 and 20,
285 respectively with Tolerance for a hotspots matching algorithm for docking ligands set to 0.25;
286 Maximum Number of Hits which defines the maximum number of hits saved for each ligand during
287 hotspots matching prior to final pose minimization was set to 100 with Final Score Cutoff, i.e.
288 fragment of the reported top scoring poses set to 0.5; Maximum number of poses to be kept per
289 conformation was set to 30 with Maximum number of conformations for each ligand set to 1000;
290 Steric Fraction specifying the number of clashes before the pose-hotspot alignment is discontinued
291 was set to 0.10 inside the 0.5 \AA Final Cluster Radius; maximum values for the Apolar SASA Cutoff
292 and Polar SASA Cutoff were set to 15.0 \AA and 5.0 \AA , respectively. Lastly, a simulated annealing
293 refinement was performed.

294

295

296

297 *2.6. Statistical analysis*

298 All studies were performed in two to three independent experiments. Data from all experiments were
299 analyzed and related calculations done using Microsoft Office Excel 2007 and GraphPad Prism 5 for
300 Windows for statistical analysis, respectively. Data from Oatp1d1 transport activity measurements

301 are expressed in percentages of LY uptake. Concentration-dependent LY uptake was calculated by
302 using the equation (1):

303

$$304 \quad (1) \quad I_i = ((F_i - F_m) / (F_c - F_m)) \times 100$$

305

306 where I_i is the percentage of inhibition for the test concentration i , F_i is the mean fluorescent value
307 for test concentration i , F_m is the mean fluorescent value for mock and F_c is the mean fluorescent
308 value for control. Serial dilutions of the test compounds were log transformed and results were
309 analyzed by non-linear regression method used for obtaining dose-response curves, with 95%
310 confidence intervals (CI). When possible and justified with respect to the intensity of the response,
311 IC_{50} values that designate the concentrations that cause 50% of maximal observed inhibition were
312 calculated from sigmoidal dose-response curves using the equation (2):

313

$$314 \quad (2) \quad y = b + (a - b) / (1 + 10^{((LogIC_{50} - x) * h)})$$

315

316 where y is the response, b is the minimum (bottom) of response, a represents the maximum (top)
317 response, hillslope (h) is the slope of the curve, $LogIC_{50}$ is the halfway response from bottom to top
318 and x is the logarithm of inhibitor concentration.

319 For Michaelis-Menten experiments, the obtained kinetic parameters, K_m and V_{max} values were
320 calculated using the Michaelis–Menten equation (3),

321

$$322 \quad (3) \quad V = (V_{max} \times [S]) / ([S] + K_m)$$

323

324 where V is the velocity (nanomoles of substrate per microgram of proteins per minute), V_{max} is the
325 maximal velocity, $[S]$ is the substrate concentration (micromoles) and K_m is the Michaelis-Menten
326 constant. Data obtained were fitted using nonlinear regression analysis with GraphPad Prism.

327 For construction of Lineweaver-Burk plots (or double reciprocal), equation (4) was used:

328

$$329 \quad (4) \quad 1/V = K_m / V_{max} (1 / [S]) + 1 / V_{max}$$

330

331 The plots are graphical representation of the of Oatp1d1-mediated transport kinetics, with y-axis
332 intercept as $1/V_{max}$ and x-axis intercept as $-1/K_m$. The type of inhibition was determined with
333 analysis of lines convergence. Intersecting lines that converge at the y-axis indicate the competitive
334 inhibition modality, whereas intersecting lines that converge to the left of the y-axis and on the x-axis
335 indicate noncompetitive inhibition modality (Copeland, 2005).

336

337 3. Results

338 3.1. Strength of interaction of tested MCs with zebrafish Oatp1d1 uptake transporter

339 In the first step of our study we tested the strength of interaction of six selected MC congeners towards
340 the zebrafish Oatp1d1 transporter, as determined by the inhibition of uptake of model Oatp1d1
341 substrate Lucifer yellow (LY) in transiently transfected HEK293 FlpIn/Oatp1d1 cells. As can be seen
342 on Fig. 1, the tested MC congeners markedly differed in their potency to inhibit LY transport. Apart
343 from MC-RR, all other congeners significantly inhibited LY uptake in transiently transfected cells
344 upon a short, 5 min co-exposure with LY. The most potent interactors were MC-LW and -LF that
345 resulted in an almost complete inhibition of LY uptake in transfected cells (95 and 82 %, respectively)
346 with IC_{50} values of 0.21 and 0.26 μ M, respectively. Significant inhibitory potency was also
347 determined for MC congeners -LA, -LR and -YR, resulting in 38%, 20% and 16% inhibition of LY
348 transport, respectively (Fig. 1).

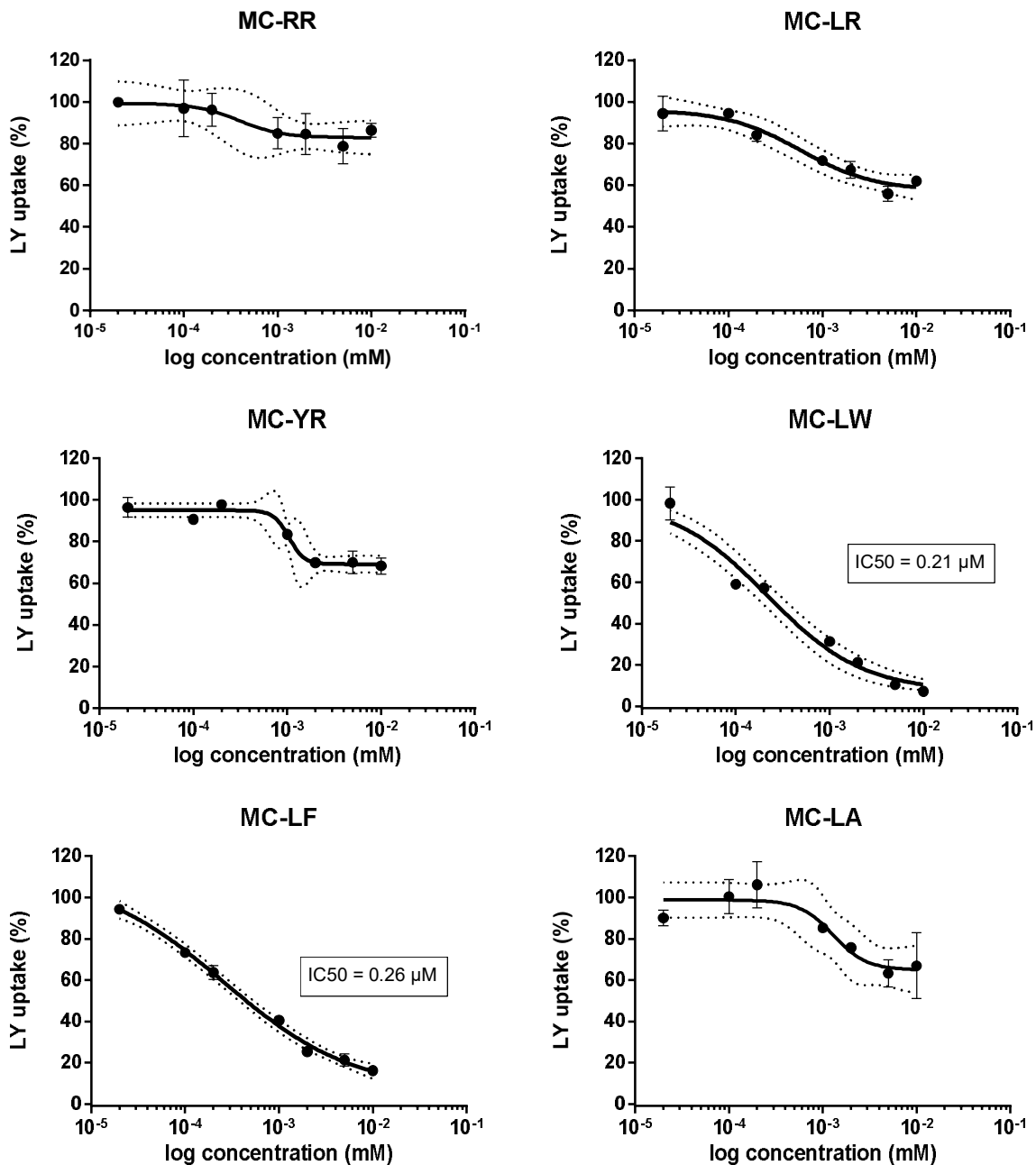
349

350 3.2. Determining the type of interaction of tested MCs with zebrafish Oatp1d1 uptake transporter

351 Michaelis-Menten transport kinetics.

352 All five MCs initially shown to interact with zebrafish Oatp1d1 with varying potency were further
353 tested for their type of interaction. Our primary goal was to discern between substrates and inhibitors
354 of zebrafish Oatp1d1, and in order to obtain more robust data and decrease variability among
355 experiments that is often present when using transient expression protocols, related experiments were
356 performed using HEK293 Flp-In cells stably overexpressing zebrafish Oatp1d1 (HEK293 Flip-
357 In/Oatp1d1) instead of the transient transfection protocol used for the initial determination of the
358 interaction strength.

359 Determinations of the type of interaction with zebrafish Oatp1d1 performed indirectly, using
360 Michaelis-Menten transport kinetics experiments. Our data showed a clear pattern of K_m increase and
361 no significant changes in V_{max} for MC congeners -LW and -LF, revealing that they are competitive
362 inhibitors of LY transport mediated by zebrafish Oatp1d1. Data were less conclusive for congener -
363 LA. Although the same pattern of the K_m increase was nominally obtained, suggesting a competitive
364 inhibition, both Michaelis-Menten kinetics (Fig. 2) and Lineweaver-Burk plots (Fig. S4) suggest
365 rather a mixed type of inhibition. On the contrary, MC-LR and -YR appeared not to be zebrafish
366 Oatp1d1 substrates as they rather acted as un-competitive inhibitors, showing a decrease in both K_m
367 and V_{max} values (Table 1, Fig. 2). Yet, we have to note that in terms of statistical robustness, data for
368 MC-LR were relatively weak, as a nominal decrease in K_m was not statistically significant with
369 respect to data obtained for MC-LR at a 10 μ m concentration. This indicates that non-competitive
370 inhibition (characterized by no changes in K_m and decrease in V_{max}) could also have been a likely
371 explanation.

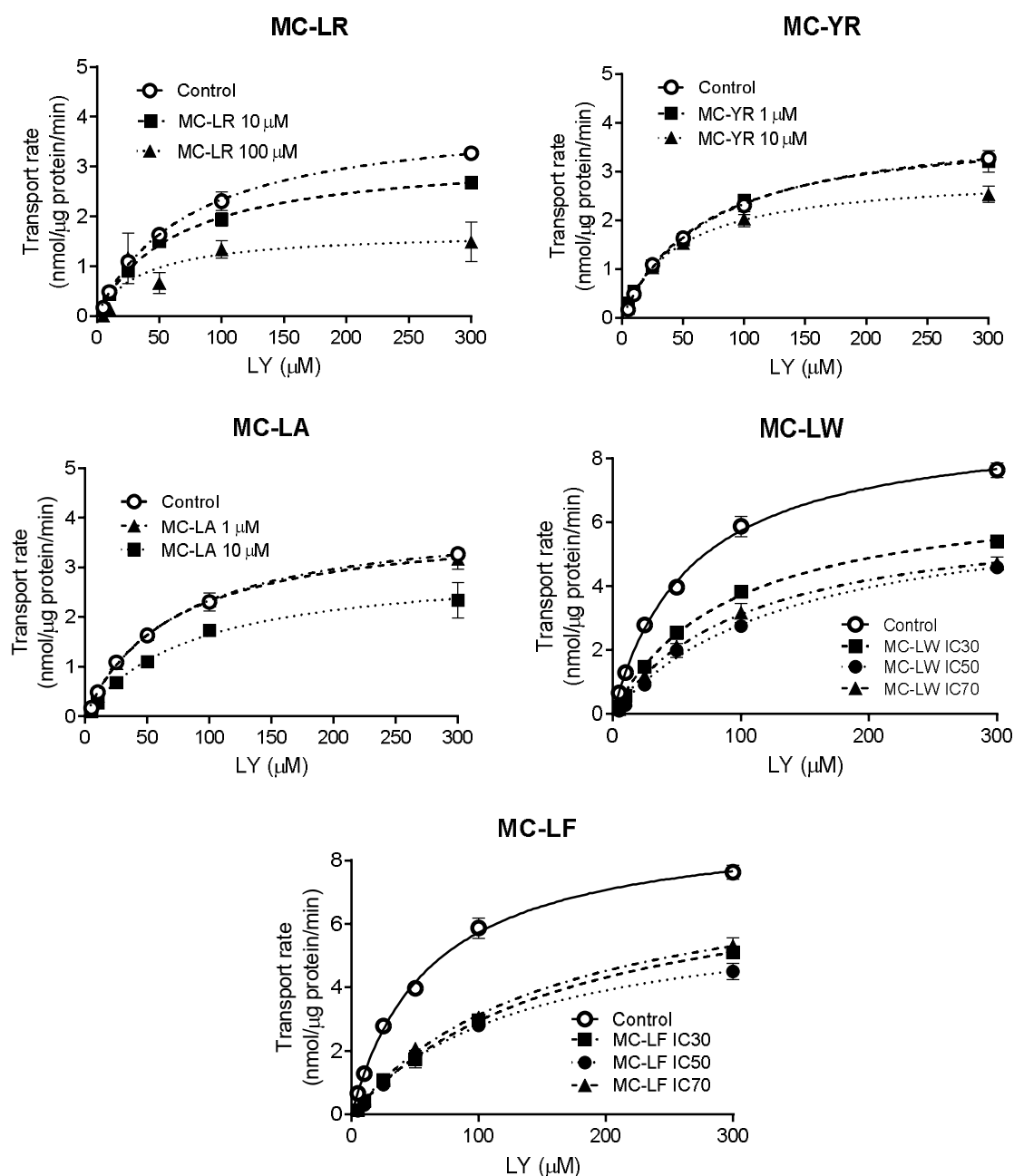


372

373

374 **Fig. 1.** Concentration-dependent inhibition of zebrafish Oatp 1d1 transport activity by MC congeners
 375 -RR, -LR, - YR, -LW, -LF and -LA. Results from a typical experiment are shown as percentages of
 376 LY uptake in HEK 293 FlpIn/Oatp1d1 cells. Each data point represents the mean \pm SD from a typical
 377 experiment out of three independent determinations. Dotted lines represent 95 % confidence intervals.

378



379

380

381 **Fig. 2.** Michaelis-Menten kinetics of zebrafish Oatp 1d1 mediated uptake of model fluorescent

382 substrate LY in the presence of MC congeners -LR, -YR, LA, -LW and -LF as determined in HEK

383 293 Flp In/Oatp1d1 overexpressing cells. Dose response curves show concentration dependence of

384 Oatp1d1 mediated LY uptake expressed as transport rate (nmol/μg protein/min) over LY

385 concentration after 15 min incubation at 37 °C in the presence of increasing concentrations of tested

386 congeners, as explained in Materials and Methods section. The concentration range of LY was from

387 5-300 μM. The uptake into vector transfected HEK 293 cells (mock-transfected cells) was subtracted

388 to obtain a transporter specific uptake. Each data point represents the mean ± SD from a typical

389 experiment out of three independent determinations.

390

391 **Table 1.** Determination of the type of interaction of the tested MC congeners with zebrafish Oatp1d1
 392 using Michaelis-Menten transport kinetics experiments. Kinetic analysis of LY transport by HEK 293
 393 Flp In/Oatp1d1 over expressing cells was determined in the absence (control) or the presence of
 394 various concentrations MC congeners, as indicated. The LY uptake followed Michaelis-Menten type
 395 kinetics, and based on the data obtained MCs were classified as substrates (competitive inhibitors) or
 396 inhibitors (non- or un-competitive) according to criteria described in Materials and Methods section.
 397 Uptake was measured after 15 min incubation at 37 °C and the results represent means \pm SEs from
 398 two (LW and LF) and three (LR, YR, LA) independent experiments performed in technical
 399 duplicates, respectively

400

MC congener	Conc. (μ M) or IC_x	$K_m \pm SE$	$V_{max} \pm SE$	Type of interaction
LR	ctrl	73.97 \pm 5.38	4.06 \pm 0.12	un-competitive inhibition
	10	63.77 \pm 14.63	3.25 \pm 0.09	
	100	47.07 \pm 12.63	1.69 \pm 0.34	
YR	ctrl	73.97 \pm 5.38	4.06 \pm 0.12	un-competitive inhibition
	1	68.47 \pm 5.7	3.95 \pm 0.13	
	10	47.20 \pm 4.25	2.95 \pm 0.09	
LA	ctrl	73.97 \pm 5.38	4.06 \pm 0.12	competitive/mixed inhibition
	1	69.47 \pm 6.24	3.92 \pm 0.14	
	10	85.24 \pm 13.86	3.95 \pm 0.20	
LW	ctrl	60.88 \pm 3.93	7.27 \pm 0.45	competitive inhibition
	IC_{30}	105.70 \pm 10.64	7.41 \pm 0.28	
	IC_{50}	111.68 \pm 5.94	7.12 \pm 0.19	
	IC_{70}	140.52 \pm 17.78	6.75 \pm 0.41	
LF	ctrl	60.88 \pm 3.93	7.27 \pm 0.45	competitive inhibition
	IC_{30}	157.8 \pm 12.84	8.09 \pm 0.32	
	IC_{50}	172.8 \pm 16.32	8.04 \pm 0.38	
	IC_{70}	135.4 \pm 13.57	7.55 \pm 0.31	

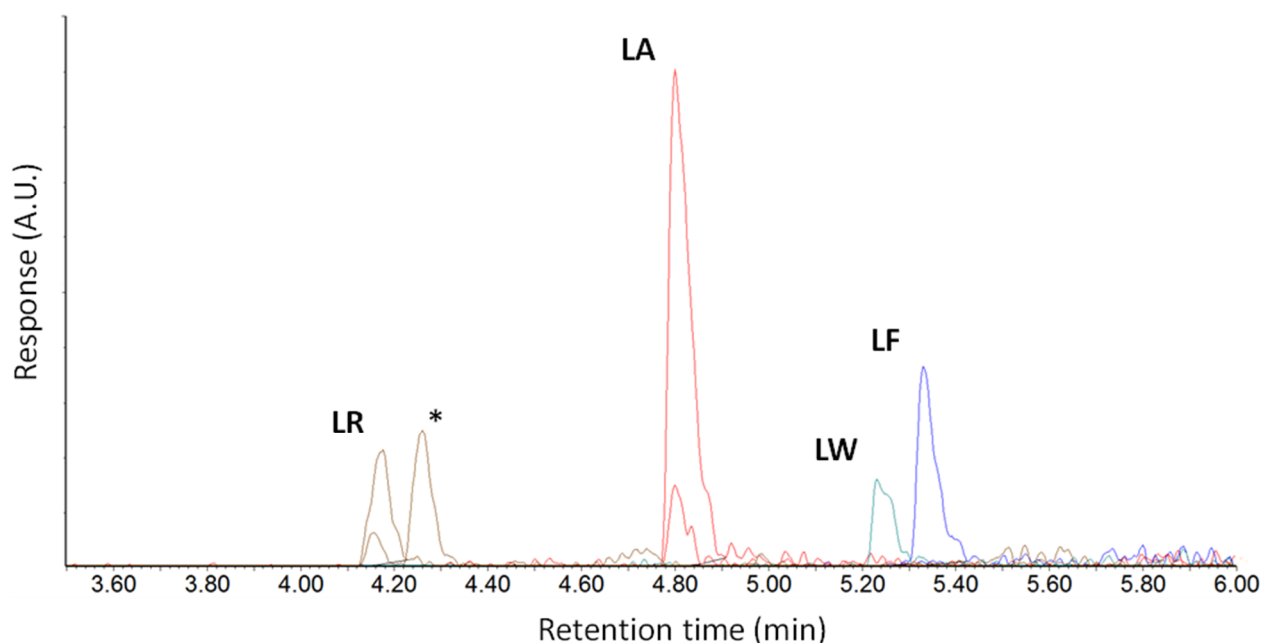
401
402

403

404 *Chemical analytical verification.* The type of interaction of the tested MC congeners with zebrafish
 405 Oatp1d1 was further verified by chemical analytical determinations of the rate of accumulation of
 406 congeners upon exposure of mock-transfected and Oatp1d1 transfected cells to increasing
 407 concentrations of the tested congeners. The result of the LC/MS analyses for the highest concentration
 408 of MCs are shown in Fig. 3, while the detailed documentation of the experiments, including all
 409 concentration levels of MCs tested, can be found in Supplementary Material (Fig. S2). The results
 410 showed significant, multi-fold increases in accumulation of MC-LA, -LF, and -LW in transfected in
 411 comparison to mock-transfected cells, confirming them as substances transported by zebrafish
 412 Oatp1d1 (Figs. 3 and 4). On the contrary, no significant Oatp1d1 mediated uptake of MC-YR was
 413 observed, confirming results of Michaelis-Menten kinetics experiments and showing that MC-YR is

414 not a zebrafish Oatp1d1 substrate. However, in contrast to data obtained by Michaelis-Menten
415 determinations, our accumulation experiments and subsequent LC-MS analysis of MC-LR showed
416 that this congener is actually transported by Oatp1d1, although at a comparatively low rate (Figs. 3
417 and 4). This suggests that MC-LR might be an Oatp1d1 substrate as well, but its transport is
418 comparatively slow.

419



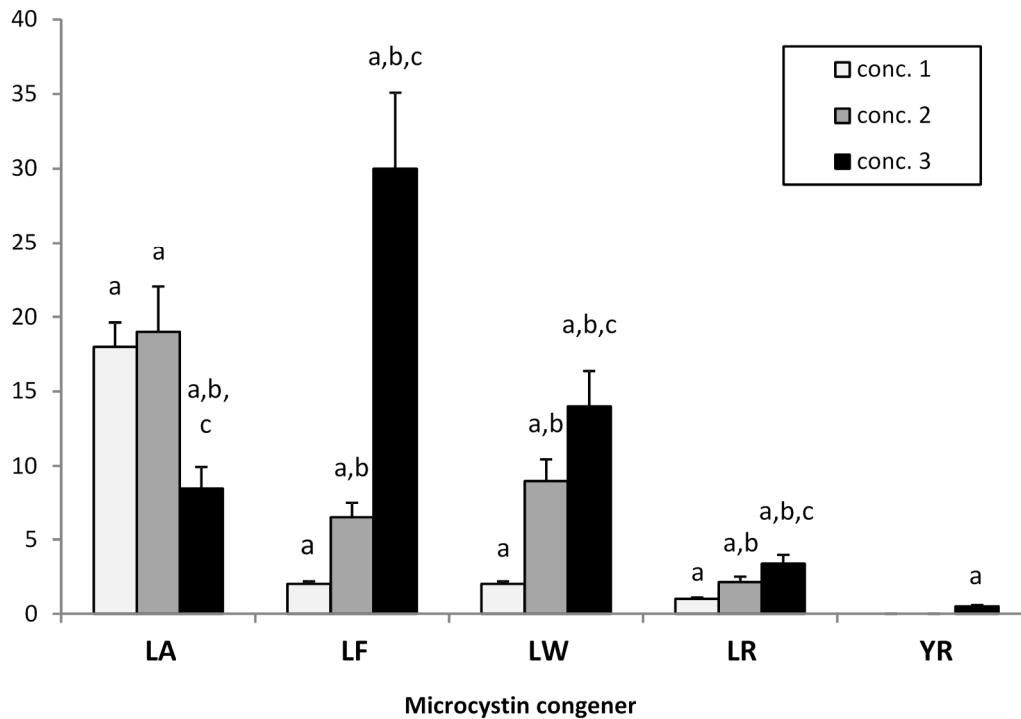
420

421 **Fig. 3.** Overlaid LC/MS chromatograms of Oatp1d1 uptake determinations with four selected
422 microcystins. The traces of individual MC congeners are given in different colors as follows: MC-
423 LR – brown, retention time (RT) 4.18 min; -LA – red, RT 4.8 min; -LW – green, RT 5.24 min; -LF
424 – blue, RT 5.33 min; *unknown impurity (RT 4.26 min). The upper and lower traces represent
425 responses obtained in Oatp1 transfected and mock-transfected cells, respectively.

426

427 3.4. Homology modelling and molecular docking studies

428 A structure-based sequence alignment of Oatp1d1 and glycerol-3-phosphate transporter template
429 from *E. coli* illustrating the unmodeled extracellular and intracellular portions (underlined) is shown
430 in the Supplementary Material (Fig. S3). Good quality alignment of the model sequence and the
431 template structure of the glycerol-3-phosphate transporter in the transmembrane regions suggested
432 that the constructed Oatp1d1 homology model should be of reasonable quality for these regions and
433 central pore description. The resulting homology model of Oatp1d1 is shown in Fig. 5. Model
434 complexes of structural model of Oatp1d1 and MCs of interest were generated using flexible
435 molecular docking where selected residues were allowed to rotate during procedure and the binding
436 sphere ($r=25 \text{ \AA}$) was defined large enough to encompass the majority of the central pore.



438

439

440

441

442

443

444

445

446

447

448

449

450

451

452

453

454

455

456

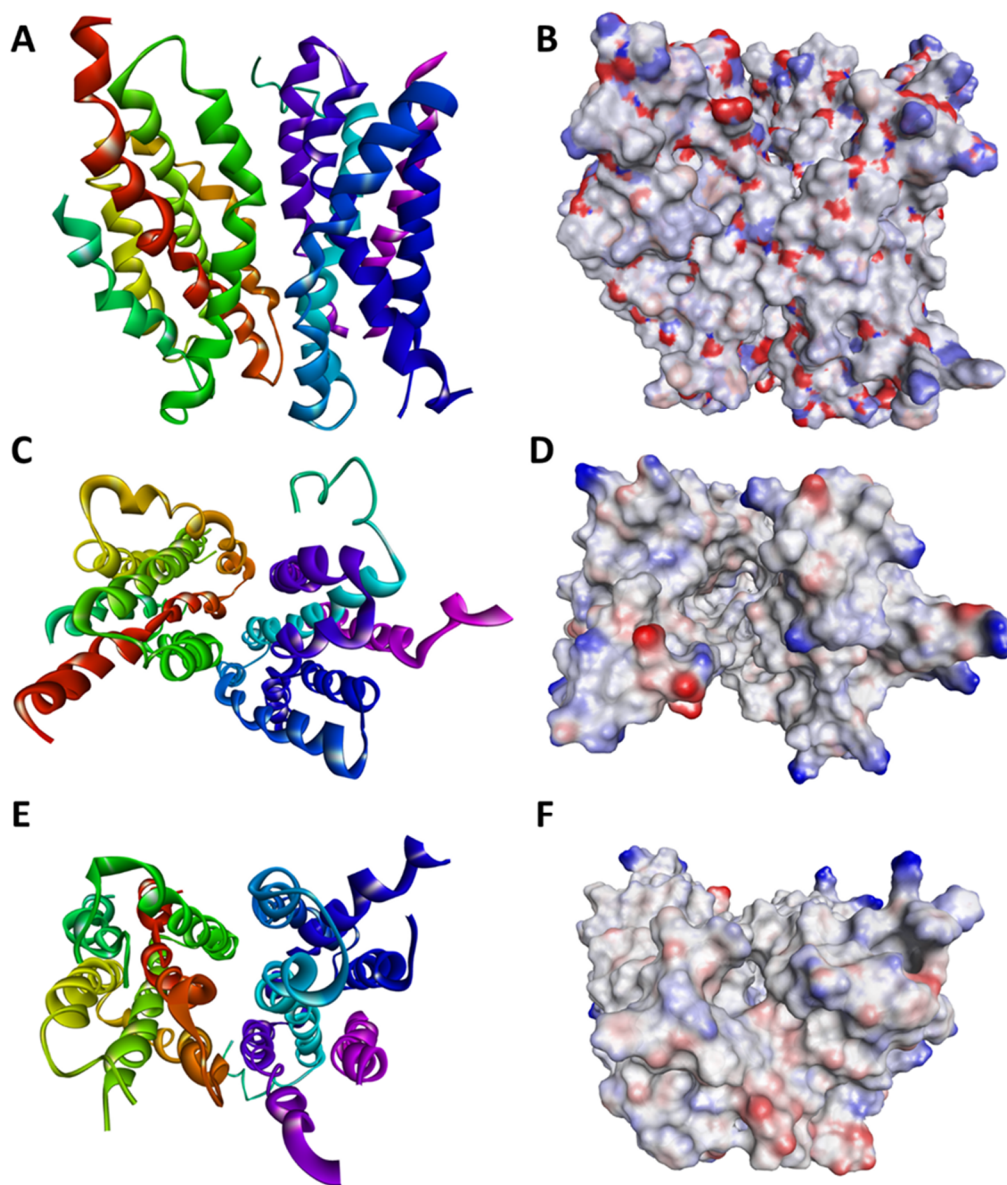
457

458

Fig. 4. Comparison of the uptake of the tested MC congeners in Oatp1d1 transfected over mock-transfected HEK293T cells. The cells were exposed to three increasing concentrations of MC congeners (0.1, 0.5 and 1 μ M for MC-LW and -LF; 0.5, 1 and 5 μ M for MC-LA and -YR; 5, 20 and 50 μ M for MC-LR) for 30 min and the amount of accumulated MCs determined using LC-MS analysis, as described in the Materials and Methods section. Data from a typical experiment are shown as means \pm SDs from triplicate determinations and represent a fold increase in the accumulation of MC congeners over the accumulation determined in mock-transfected cells for each of the three tested concentrations. One-way ANOVA and Tukey's multiple comparison test were used for determination of statistically significant differences between the uptake of corresponding MC congeners in transfected over mock-transfected cells, as well as among the uptake determined in the cells exposed to different concentrations of the same MC congener: a – significantly different ($p < 0.05$) from accumulation in mock-transfected cells; b – significantly different ($p < 0.05$) from concentration 1 of the same MC congener; c – significantly different ($p < 0.05$) from concentration 2.

However, prior to the docking study of MCs, to validate the receptor molecule, i.e. Oatp1d1 homology model, a docking of the known model substrate LY was attempted. The successful docking predicted that LY is buried deep in the central pore approximately at its center (Fig. 6AB). The five MCs that showed significant interaction with zebrafish Oatp1d1, MC-LF and MC-LW were successfully docked without any translation of the binding site. The resulting model complexes are shown in Fig. 6C-F together with the non-bonding interactions of docked MCs with neighboring

459 amino acid residues. MC-LF was predicted to be placed above the center of the pore interacting non-
460 covalently with neighboring residues identified as Ser567, Val179, Met180, Arg192, Asn195, Leu324
461 and Ser567. On the other hand, MC-LW was placed on the outer part of the sphere/central pore and
462 exposed to the surrounding fluid. In doing so, MC-LW was engaged in non-bonding interactions with
463 the following residues: Ile70, Ile203, Lys319, Lys321, and Leu575. However, the other congeners
464 failed to fully accommodate inside the defined binding sphere without significant translation of the
465 binding site sphere's center closer to the opening of the central pore. After the refinement of the
466 model, the initially failed MC congeners -LA and -LR were successfully docked. The model complex
467 between Oatp1d1 structural model and MC-LR depicts the blocking of the central pore unit by MC-
468 LR (Fig. 6GH). The binding position of MC-LR was secured through non-bonding interactions with
469 residues Met180, Leu184, and Ile55.
470



471
472 **Fig. 5.** Solid ribbon and rainbow-colored representation of the homology model of Oatp1d1 as viewed
473 from the lateral side (A), the extracellular side (C) and the intracellular side (E) with electrostatic

474 potential mapped onto its molecular surface, respectively (B, D, F). Regions of negative, positive and
475 neutral potential are shown in red, blue and white/gray, respectively. The model is deposited and
476 available at ModelArchive base (<https://www.modelarchive.org/doi/10.5452/ma-4kkal>).

477

478 **4. Discussion**

479 Based on the studies published so far, the uptake kinetics of various MC congeners is a factor that
480 largely determines their bioavailability and toxic potential in exposed aquatic organisms, and Oatp
481 transporters appeared to be major contributors relevant for the uptake of MCs in fish species (Meier-
482 Abt et al., 2007; Bury et al., 1998; Bieczynski et al., 2014; Faltermann et al., 2016; Steiner et al.,
483 2016). Yet, more detailed studies performed recently utilizing zebrafish as a cyprinid fish model
484 showed that the rate of MC uptake significantly varies for different congeners. Furthermore, it has
485 been shown that zebrafish Oatp1d1 acts as a ubiquitously expressed, multi-specific transporters of
486 various MC congeners, while other MC transporting Oatps, like members of the Oatp1f subfamily,
487 are expressed exclusively in the kidney and transport only specific MC congeners (Steiner et al.,
488 2015). As the primary cause for this variability could be related to the strength and type of interaction
489 (substrates versus inhibitors) of MC congeners with fish Oatp1d1 transporter, it is logical to assume
490 that these features may contribute to differences in the toxic potential of individual congeners towards
491 fish species as one of the primary targets of cyanotoxins and subsequent toxic effects related to HABs.
492 Therefore, it is highly relevant to better characterize the MC congeners frequently found in HABs
493 with respect to their interaction with Oatp1d1. To do so, we selected six MC congeners that differ in
494 terms of various structural properties and their log P_{OW} values (Table S1) and utilized HEK293T cells
495 transiently or stably expressing zebrafish Oatp1d1 as a specific and sensitive assay system for testing
496 their interaction with this transporter.

497 In the first part of our study, we determined the strength of interaction of the tested MCs and found
498 that most of them do interact with zebrafish Oatp1d1, inhibiting the uptake of model Oatp1d1
499 substrate LY in transfected cells with varying potency. What was immediately obvious was that the
500 strongest interactors were also the most lipophilic congeners -LW and -LF (Fig. 1), followed by
501 congeners -LA, -LR and -YR, again in apparent correlation with their log P_{OW}. Furthermore, as the
502 only truly hydrophilic congener, with log P_{OW} value of -0.2, MC-RR did not significantly interfere
503 with LY transport by Oatp1d1. These results were similar to data reported earlier by Steiner et al.
504 (2015), with the exception of MC-RR that was shown to be transported by zebrafish Oatp1d1, albeit
505 at a slow rate and as the result of a prolonged 24 h exposure.

506 However, our initial data on the interaction strength, although specific enough due to the use of
507 Oatp1d1 overexpressing cells, could not reveal if the tested MC congeners are substances transported
508 by the zebrafish Oatp1d1 transporter, or they inhibit LY transport due to an un- or non-competitive
509 mode of inhibition. To get a better insight into the type of interaction, in the next step of our study

510 we performed Michaelis-Menten kinetics determinations of the type of interaction for five MC
511 congeners shown to be Oatp1d1 interactors. Although Michaelis-Menten kinetics measurements are
512 not a direct determination of substrate transport, we utilized it as an established experimental protocol
513 to discern between substrates and inhibitors and showed that MC-LW and -LF clearly behaved as
514 substrates (i.e. competitive inhibitors), while congeners -LR and -YR appeared not to be transported
515 by Oatp1d1. (Table 1, Figs. 2 and S4). Considering the robustness of the data in respect to the
516 calculated K_m and V_{max} values for LY transport, and their shifts in comparison to control values
517 determined without addition of the tested MC congeners, the data obtained using this method
518 appeared to be a good indication of congeners that are substrates versus those that act as Oatp1d1
519 inhibitors. The exceptions were MC-LA that were less conclusive and showed a mixed inhibition
520 pattern, and MC-LR where in terms of statistical robustness the data were relatively weak, as a
521 nominal decrease in K_m was not statistically significant with respect to data obtained for MC-LR at
522 10 μm concentration (Table 1, Figs. 2 and S4). This indicates that non-competitive inhibition
523 (characterized by no changes in K_m and a decrease in V_{max}) could also have been a likely
524 explanation.

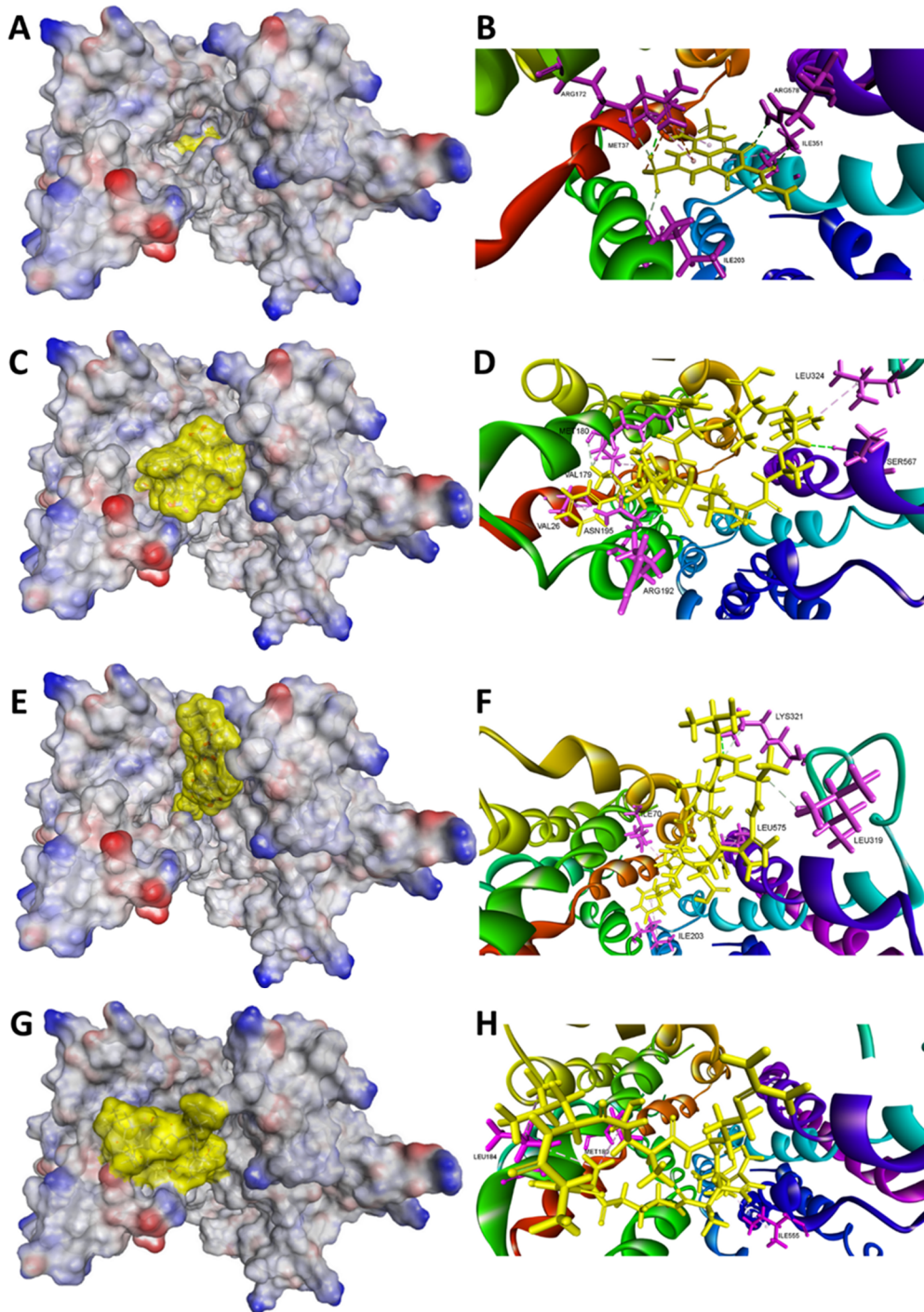
525 In addition to Michaelis-Menten kinetics data, the transport of selected MCs by zebrafish was further
526 studied by direct chemical analytical determination of their accumulation rate in transfected and
527 mock-transfected cells by LC-MS analysis. The obtained results were rather consistent with the
528 results of kinetics determinations: significant increases in accumulation of MC-LF, -LW, and -LA
529 were determined in transfected over mock-transfected cells at all of the three concentrations of MCs,
530 confirming them as substrates for zebrafish Oatp1d1 (Figs. 3, 4 and S2). Likewise, exposure to MC-
531 YR did not result in a significant fold-increase in accumulation over mock-transfected cells, showing
532 that MC-YR was not transported by Oatp1d1. Yet, two irregularities were shown. The first is related
533 to the lack of consistent dose response for MC-LA, where the exposure of the cells to the highest
534 concentration actually resulted in lower accumulation of MC-LA in comparison to the two lower
535 concentrations (Fig. 4). A likely explanation for this discrepancy might be related to suboptimal range
536 of the concentrations used. For example, although MCs interact with cellular PPs primarily by non-
537 covalent, two-step mechanism involving rapid binding and inactivation of PPs, the process is
538 followed by a slower (within hours) covalent interaction (Craig et al., 1996; Hastie et al., 2005;
539 Perreira et al., 2011). However, although a shorter, 30 min methanol extraction protocol was used in
540 our study, it is possible that a more significant covalent interaction happened at the highest MC-LA
541 concentration used, partly preventing extraction of accumulated MC-LA by methanol. Nevertheless,
542 even at that concentration the accumulation of MC-LA was clearly much higher in transfected over
543 mock-transfected cells showing basically that -LA congener is also a substrate transported by
544 zebrafish Oatp1d1.

545 Second inconsistency was related to MC-LR data. In contrast to partially inconclusive Michaelis-
546 Menten analysis of MC-LR kinetics, chemical analytical determinations showed that MC-LR was
547 transported into Oatp1d1 overexpressing cells, although at a lower rate (Figs. 3, 4, S2 and S4). These
548 data are actually in agreement with previous reports that showed that MC-LR is an Oatp1d1 substrate
549 in zebrafish (Steiner et al., 2015; Faltermann et al., 2016). In terms of LC-LR toxicokinetics, the
550 detailed study by Steiner and colleagues (2015) is particularly relevant, as it showed that intracellular
551 transport of MC-LR by Oatp1d1 is much less favorable when compared to transport of more
552 hydrophobic congeners like -LW or -LF, which are transported much faster. Consequently, although
553 the authors correctly pointed out that kinetic values obtained in various studies using different
554 exposure regimes, model substrates and/or detection methods should not be directly compared, we
555 believe the overall pattern determined in our study is quite consistent with previous reports, which
556 indicates that MC-LR is a slow, low affinity substrate for Oatp1d1 transporter.

557 Finally, to confirm experimentally observed different modes of action among the tested compounds,
558 a structural study was undertaken utilizing molecular modelling. Since a crystal structure of zebrafish
559 Oatp1d1 is not available, a homology model was constructed based on a chosen template crystal
560 structure of the glycerol-3-phosphate transporter from *E. coli* solved in a conformation with the
561 central pore opening toward the intracellular side (F. Meier-Abt et al., 2006, Huang et al., 2003).
562 Although the used template structure was not ideal in terms of the sequence similarity (Fig. S3), and
563 long insertions that could not be modelled correctly were excised from the alignment in order to
564 obtain a reliable model, all of the excised insertions were either from the N-terminal region or large
565 extracellular/intracellular loops/regions not important for ligand binding. As a result, the final
566 alignment of the model sequence and the template structure was of substantial quality, implying that
567 the Oatp1d1 homology model constructed (Fig. 5) could be used for reliable molecular docking
568 studies. It was further confirmed by successful docking of LY as a verified substrate for zebrafish
569 Oatp1d1, which was docked deep in the central pore of zebrafish Oatp1d1 (Fig. 6AB). Moreover, LY
570 was predicted to interact with Met37 via a hydrophobic π -alkyl non-covalent bond, and this residue
571 corresponds to the position of Arg45 in the model glycerol-3-phosphate transporter described as one
572 of the key residues for substrate binding, located at the closed end of the substrate-translocation
573 pathway in the middle of the membrane (Huang et al., 2003).

574 As to the docking studies of MC congeners, although all five MCs were studied and the most potent
575 interactors MC-LF and MC-LW were successfully docked, others initially failed to fully
576 accommodate inside the defined binding sphere. Such an outcome could have been expected for MC-
577 YR, which was shown both indirectly (Michaelis-Menten kinetics) and directly (chemical analytical
578 determinations) not to be transported by zebrafish Oatp1d1, but the docking of MC-LA and -LR
579 inside the Oatp1d1 central pore, however, was expected. Nevertheless, after the refinement of the
580 model by translation of the binding site sphere's center closer to the opening of the central pore, MC-

581 LA and -LR were successfully docked. Interestingly, it can be seen that MC-LR is placed higher
582 above the central pore when compared with the predicted binding pose of MC-LF, and bulky MC-
583 LR is clearly prevented from easily entering the central pore.
584



585
586 **Fig. 6.** Electrostatic potential mapped on the molecular surface of model complexes between
587 structural model of Oatp1d1 and LY (A), MC-LF (C), MC-LW (E), or MC-LR (G). Regions of
588 negative, positive and neutral potential are shown in red, blue and white/gray, respectively. The
589 molecular surface of ligands is shown in yellow. The close-up of LY (B), MC-LF (D), MC-LW (F),
590 or MC-LR (H) docked into the central pore of the structural model of zebrafish Oatp1d1. The ligands

591 are shown in yellow sticks and amino acid residues engaged in non-bonding interactions (dotted lines)
592 are shown in magenta sticks.

593

594 Furthermore, although no crystal structures of the OATPs/Oatps are available and the transport
595 mechanism of OATPs/Oatps has not been fully elucidated, the available *in silico* models imply that
596 transport of their substrates most probably occur through a central, positively charged pore (Meier-
597 Abt et al., 2005). Consequently, as Oatps are primarily anion transporters, the presence of positively
598 charged arginine residues in MC-LR, -YR, and -RR probably contributed to its lower affinities
599 towards zebrafish Oatp1d1. Considering the strength and type of interaction of tested MCs versus
600 their physicochemical descriptors, our data support earlier observations (Karlgrén et al., 2012;
601 Wolman et al., 2013) which indicated that apart from lipophilicity, properties like topological polar
602 surface area and hydrogen bond features correlate with the potency of various substances, including
603 MCs (Table S1), for interaction with OATPs/Oatps, including zebrafish Oatp1d1.

604

605 **5. Conclusion**

606 Taken together, the data obtained in this study support results by similar studies implying that the
607 zebrafish Oatp1d1 is a membrane transporter that could be a rate limiting step for the uptake of
608 microcystins in cyprinids, and possibly other teleosts. However, although a wide substrate
609 preference and a rather large binding region of zebrafish Oatp1d1 do enable the transport of
610 structurally and chemically different MC congeners, it seems to be highly plausible that the transport
611 of MCs could be largely dependent on their basic physicochemical properties, with log P_{OW} being the
612 most obvious determinant.

613 Secondly, as previously suggested by Stainer et al. (2015), the presence of nominally highly toxic
614 MC congeners (e.g., MC-LR) in cyanobacterial blooms does not necessarily translate to high
615 ecological risk if their capacity for Oatp1d1 transport is low. And vice versa, the presence of
616 nominally less toxic MCs (e.g., MC-LF or -LA) that are in contrast readily taken up by Oatp1d1 can
617 result in highly relevant deleterious effects in exposed fish, especially neurotoxicity and renal toxicity
618 in organs and tissues characterized by significant expression of Oatp1d1 or related transporters with
619 overlapping substrate specificities.

620 Consequently, apart from the determination of chemical composition of HABs in relation to MCs, a
621 reliable risk assessment should take into account the interaction of identified MC congeners with
622 Oatp1d1 as their primary transporter in fish species. As demonstrated, the use of highly specific *in*
623 *vitro* models in combination with uptake and kinetics determinations, chemical analytical verification
624 and *in silico* molecular docking studies could be used as a reliable experimental setup for this goal.

625 **Acknowledgements**

626 This research was financed by the Croatian Science Foundation (Project No. IP-2019-04-1147) and
627 partially supported under the STIM-REI project, Contract Number: KK.01.1.1.01.0003, a project
628 funded by the European Union through the European Regional Development Fund – the Operational
629 Programme Competitiveness and Cohesion 2014–2020 (KK.01.1.1.01). The computational resources
630 and Biovia Discovery Studio Client v18.1 software (Dassault Systèmes, Vélizy-Villacoublay,
631 France), used for homology modeling and molecular docking studies, were provided through Croatian
632 Science Foundation projects (grant numbers HrZZ-IP-2013-11-4307 and HrZZ-IP-2018-01-7683).

633 *Author contributions:* PM – designed and performed majority of interaction and exposure
634 experiments related to chemical analytical determinations, and wrote the manuscript; MA – LC-MS
635 determinations; NM – homology modelling and molecular docking studies; JL and IM – performed
636 part of Michaelis-Menten kinetics studies; TS – supervision of the project, study conception and
637 design, writing of the paper with input from all authors. All of the authors reviewed the results and
638 approved the final version of the manuscript.

639

640 **Abbreviations:** MC – microcystin; OATP/Oatp – organic anion-transporting polypeptide; HAB –
641 harmful algal bloom; LY – Lucifer yellow; HEK293T - human embryonic kidney cells; LC-MS –
642 liquid chromatography-mass spectrometry; QTOF-MS – quadrupole-time-of-flight/mass
643 spectrometry; TIC – total ion current; UPLC – ultra-performance liquid chromatography.

644

645 **References**

- 646 1) Sivonen, K., Jones, G. Cyanobacterial toxins. In: Chorus I, Bartram J, editors. Toxic
647 Cyanobacteria in Water: A Guide to Public Health Significance, Monitoring and Management.
648 London: E&FN Spon; 1999. pp. 41–111.
- 649 2) Dittmann, E., Fewer, D.P., Neilan, B.A., 2013. Cyanobacterial toxins: biosynthetic routes and
650 evolutionary roots. FEMS Microb. Rev. 37, 23-43.
- 651 3) D'Anglada, L.V., Hilborn, E.D., Backer, L.C. (Eds.). Harmful Algal Blooms (HABs) and Public
652 Health: Progress and Current Challenges. Toxins special edition, 2016 MDPI Books.
- 653 4) Wang, H., Xu, C., Liu Y., Jeppesen, E., Svenning, J.C., Wu, J., Zhang, W., Zhou, T., Wang, P.,
654 Nangombe, S., Ma, J., Duan, H., Fang, J., Xie, P. 2021. From unusual suspect to serial killer:
655 Cyanotoxins boosted by climate change may jeopardize megafauna. The Innovation 2(2),
656 100092.
- 657 5) Zohdi, E., Abbaspour, M., 2019. Harmful algal blooms (red tide): a review of causes, impacts
658 and approaches to monitoring and prediction. Int. J. Environ. Sci. Technol. 16, 1789-1806.
- 659 6) Ferrão-Filho Ada, S., Kozłowsky-Suzuki, B., 2011. Cyanotoxins: bioaccumulation and effects
660 on aquatic animals. Mar Drugs. 9, 2729-2772.

- 661 7) Buratti, F.M., Manganelli, M., Vichi, S., Stefanelli, M., Scardala, S., Testai, E., Funari, E., 2017.
662 Cyanotoxins: producing organisms, occurrence, toxicity, mechanism of action and human health
663 toxicological risk evaluation. Arch. Toxicol. 1, 1049-1130.
- 664 8) Chen, J., Xie, P., Li, L., Xu, J. 2009. First identification of the hepatotoxic microcystins in the
665 serum of a chronically exposed human population together with indication of hepatocellular
666 damage. Toxicol. Sci. 108, 81-89.
- 667 9) Bouaïcha, N., Miles CO, Beach DG, et al. Structural Diversity, Characterization and Toxicology
668 of Microcystins. Toxins 2019, 11, 714.
- 669 10) Craig, M., Luu, H.A., McCready, T.L., Holmes, C.F.B., Williams, D., Andersen, R.J. 1996.
670 Molecular mechanisms underlying the interaction of motuporin and microcystins with type-1 and
671 type-2A protein phosphatases. Biochem. Cell Biol. 1996, 74, 569–578.
- 672 11) Hastie, C., Borthwick, E., Morrison, L., Codd, G., Cohen, P. 2005. Inhibition of several protein
673 phosphatases by a non-covalently interacting microcystin and a novel cyanobacterial peptide,
674 nostocyclin. BBA Gen. 1726, 187–193.
- 675 12) Pereira, S.R., Vasconcelos, V.M., Antunes, A. 2011. The phosphoprotein phosphatase family of
676 Ser/Thr phosphatases as principal targets of naturally occurring toxins. Crit. Rev. Toxicol. 41,
677 83–110.
- 678 13) MacKintosh C, Beattie, K.A., Klumpp, S, Cohen, P., Codd, G.A., 1990. Cyanobacterial
679 microcystin-LR is a potent and specific inhibitor of protein phosphatases 1 and 2A from both
680 mammals and higher plants. FEBS Lett. 264, 187-192.
- 681 14) McLellan, N.L., Manderville, R.A., 2017. Toxic mechanisms of microcystins in mammals.
682 Toxicol. Res. (Camb).6, 391-405.
- 683 15) Fischer, A., Hoeger, S.J., Stemmer, K., Feurstein, D.J., Knobloch, D., Nussler, A., Dietrich,
684 D.R., 2010. The role of organic anion transporting polypeptides (OATPs/SLCOs) in the toxicity
685 of different microcystin congeners *in vitro*: A comparison of primary human hepatocytes and
686 OATP-transfected HEK293 cells. Toxicol. Appl. Pharmacol. 245, 9-20.
- 687 16) Niedermeyer, T.H.J., Daily, A., Swiatecka-Hagenbruch, M., Moscow, J.A., 2014. Selectivity and
688 potency of microcystin congeners against OATP1B1 and OATP1B3 expressing cancer cells. Plos
689 ONE, 9, e91476.
- 690 17) Steiner, K., Zimmermann, L., Hagenbuch, B., Dietrich, D., 2015. Zebrafish Oatp-mediated
691 transport of microcystin congeners. Arch. Toxicol. 90, 1129-1139.
- 692 18) Hagenbuch, B., Meier, P.J., 2003. The superfamily of organic anion transporting polypeptides.
693 Biochim. Biophys. Acta – Biomem. 1609, 1-18.
- 694 19) Popovic, M., Zaja, R., Smital, T., 2010. Organic anion transporting polypeptides (OATP) in
695 zebrafish (*Danio rerio*): Phylogenetic analysis and tissue distribution. Comp. Biochem. Physiol.
696 A Mol. Integr. Physiol. 155, 327-335.

- 697 20) Fischer, W.J., Altheimer, S., Cattori, V., Meier, P.J., Dietrich, D.R., Hagenbuch, B., 2005.
698 Organic anion transporting polypeptides expressed in liver and brain mediate uptake of
699 microcystin. *Toxicol. Appl. Pharmacol.* 203, 257-263.
- 700 21) Komatsu, M., Furukawa, T., Ikeda, R., Takumi, S., Nong, Q., Aoyama, K., Akiyama, S., Keppler,
701 D., Takeuchi, T., 2007. Involvement of mitogen-activated protein kinase signaling pathways in
702 microcystin-LR-induced apoptosis after its selective uptake mediated by OATP1B1 and
703 OATP1B3. *Toxicol. Sci.* 97, 407-416.
- 704 22) Meier-Abt, F., Hammann-Hänni, A., Stieger, B., Ballatori, N., Boyer, J.L., 2007. The organic
705 anion transport polypeptide 1d1 (Oatp1d1) mediates hepatocellular uptake of phalloidin and
706 microcystin into skate liver. *Toxicol. Appl. Pharmacol.* 218, 274-279.
- 707 23) Bury, N.R., Newlands, A.D., Eddy, F.B., Codd, G.A., 1998. *In vivo* and *in vitro* intestinal
708 transport of 3H-microcystin-LR, a cyanobacterial toxin, in rainbow trout (*Oncorhynchus mykiss*).
709 *Aquat. Toxicol.* 42, 139-148.
- 710 24) Bieczynski, F., De Anna, J.S., Pirez, M., Brena, B.M., Villanueva, S.S.M., Luquet, C.M., 2014.
711 Cellular transport of microcystin-LR in rainbow trout (*Oncorhynchus mykiss*) across the
712 intestinal wall: Possible involvement of multidrug resistance-associated proteins. *Aquat. Toxicol.*
713 154, 97-106.
- 714 25) Faltermann, S., Prétôt, R., Pernthaler, J., Fent, K., 2016. Comparative effects of nodularin and
715 microcystin-LR in zebrafish: 1. Uptake by organic anion transporting polypeptide Oatp1d1
716 (Slco1d1). *Aquat. Toxicol.* 171, 69-76.
- 717 26) Popovic, M., Zaja, R., Fent, K., Smital, T., 2013. Molecular characterization of zebrafish
718 Oatp1d1 (Slco1d1), a novel Organic anion transporting polypeptide. *J. Biol. Chem.* 288, 33894–
719 33911.
- 720 27) Marić, P., Ahel, M., Senta, I., Terzić, S., Mikac, I., Žuljević, A., Smital, T., 2017. Effect-directed
721 analysis reveals inhibition of zebrafish uptake transporter Oatp1d1 by caulerpenyne, a major
722 secondary metabolite from the invasive marine alga *Caulerpa taxifolia*. *Chemosphere* 174, 643-
723 654.
- 724 28) Lončar, J., Smital, T., 2018. Interaction of environmental contaminants with zebrafish (*Danio*
725 *rerio*) multidrug and toxin extrusion protein 7 (Mate7/Slc47a7). *Aquat. Toxicol.* 205, 193-203.
- 726 29) Bradford, M., 1976. A rapid and sensitive method for the quantification of microgram quantities
727 of protein utilizing the principle of protein-dye binding. *Anal. Biochem.* 72, 248-254.
- 728 30) Terzic, S. and Ahel, M., 2011. Nontarget analysis of polar contaminants in freshwater sediments
729 influenced by pharmaceutical industry using ultra-high-pressure liquid chromatography-
730 quadrupole time-of-flight mass spectrometry. *Environ. Pollut.* 159, 555-566.

- 731 31) Meier-Abt, F., Mokrab, Y., Mizuguchi, K., 2005. Organic anion transporting polypeptides of the
732 OATP/SLCO superfamily: identification of new members in nonmammalian species,
733 comparative modeling and a potential transport mode. *J. Memb. Biol.* 208, 213–227.
- 734 32) Yafei Huang, M. Lemieux, J., Song, J., Auer, M., Da-Neng, W., 2003. Structure and mechanism
735 of the glycerol-3-phosphate transporter from *Escherichia coli*. *Science* 301, 616–620.
- 736 33) Sali, A., Blundell, T.L., 1993. Comparative protein modelling by satisfaction of spatial restraints.
737 *J. Mol. Biol.* 234, 779-815.
- 738 34) Shen, M.Y., Sali, A., 2006. Statistical potential for assessment and prediction of protein
739 structures. *Protein Sci.* 15, 2507-2524.
- 740 35) Koska, J., Spassov, V.Z., Maynard, A.J., Yan, L., Austin, N., Flook, P.K., Venkatachalam, C.M.,
741 2008. Fully automated molecular mechanics based induced fit protein-ligand docking method. *J.*
742 *Chem. Inf. Model.* 48, 1965-1973.
- 743 36) Copeland, R.A., 2005. Evaluation of Enzyme Inhibitors in Drug Discovery, *Journal of Chemical*
744 *Information and Modeling*. A John Wiley & Sons, Inc., Hoboken, New Jersey.
745 <https://doi.org/10.1017/CBO9781107415324.004>.
- 746 37) Meier-Abt, F., Mokrab, Y., Mizuguchi, K., 2005. Organic anion transporting polypeptides of the
747 OATP/SLCO superfamily: identification of new members in nonmammalian species,
748 comparative modeling and a potential transport mode. *J. Membr. Biol.* 208, 213–227.
- 749 38) Karlgren, M., Vildhede, A., Norinder, U., Wisniewski, J.R., Kimoto, E., Lai, Y., Haglund, U.,
750 Artursson, P., 2012. Classification of inhibitors of hepatic organic anion transporting
751 polypeptides (OATPs): influence of protein expression on drug–drug interactions. *J. Med.*
752 *Chem.* 55, 4740–4763.
- 753 39) Wolman, A.T, Gionfriddo, M.R., Heindel, G.A., Mukhija, P., Witkowski, S., Bommarreddy, A.,
754 VanWert, A.L., 2013. Organic anion transporter 3 interacts eelectively with lipophilic β -lactam
755 antibiotics. *Drg. Metabol. Disp.* 41, 791-800.